iJRASET
International Journal For Research in Applied Science and Engineering Technology

INTERNATIONAL JOURNAL FOR RESEARCH

IN APPLIED SCIENCE & ENGINEERING TECHNOLOGY

Volume: 13 **Issue:** II **Month of publication:** February 2025

DOI: https://doi.org/10.22214/ijraset.2025.67108

www.ijraset.com

Call: 08813907089 | E-mail ID: ijraset@gmail.com

International Journal for Research in Applied Science & Engineering Technology (IJRASET)
ISSN: 2321-9653; IC Value: 45.98; SJ Impact Factor: 7.538
Volume 13 Issue II Feb 2025- Available at www.ijraset.com

Removal of Dye using Novel Nanoparticles with Performance, Characterization, Kinetic & Isotherm Study from Waste Water

Dharmendra Patel[1], Mahesh Patel[2], Parwathi Pillai[2*]
[1]*Department of Chemistry, Swarrnim Institute of Science, Swarrnim start-up & Innovation University, Gandhinagar 382420, India*
[2]*Department of Chemical Engineering, Swarrnim Institute of Technology, Swarrnim start-up & Innovation University, Gandhinagar 382420, India*

Abstract: ***The effluent containing dye is one of the major health concerns for humans and the environment. Iron oxide nanoparticle (Fe NPs) has properties like size, large surface area, and magnetic nature that were more impressive for removing dye from the aqueous solution. Batch adsorption tests for the removal of dye from synthetic dye water were done in the current work, and the modified iron oxide nanoparticle with rice husk ash (RH+Fe) was confirmed by characterization techniques like XRD, FTIR, SEM, and particle size analysis. Using 2.6 g/L, 50 °C, and 10 ppm of adsorbent dosage, starting concentration, and temperature of RH+Fe, 96 % of the dye was removed. The RH+Fe adsorbent data were best fitted for Langmuir isotherm and had an adsorption capacity of 98 mg*** g^{-1}***. In the kinetic investigation, the regression coefficient of pseudo-second order was determined to be 0.96. The results of the current investigation offer a promising dye elimination adsorbent.***
Keywords: Dye, Silica Nano, Rice husk, Iron oxide, Adsorption

I. INTRODUCTION

One of the most important aspects of the earth's landscape are rivers. They transport the surface water and nutrients from the sedimentation regions to the oceans. In addition to being important sources of drinking water, rivers also support marine life, which provides food for both humans and animals. Rivers are also a valuable resource in contemporary human culture because of their involvement in tourism, the production of hydroelectricity, etc. Regrettably, rivers are also conveniently used by careless people and businesses to dispose of waste items and toxins [1]. The primary threat to water security is said to be the direct release of pollutants into water bodies without sufficient treatment, coming from a variety of sources. For example, the dye business is ranked as the tenth most polluting industry to river water, contributing between 17 and 20 percent of industrial water pollution from textile dyeing and treatment. Every year, 5,000–10,000 tonnes of dyes are discharged into the waterways as a result of their widespread use2,3. Reactive Black 5 (RB5) and Congo red (CR) are two of the most widely used dyes since their introduction. These dyes are known as anionic dyes because their molecules dissociate in water with negative charges [2]. These dyes endanger the health of the aquatic ecosystem and the surrounding community when they are dumped directly into surface waters because they block sunlight, which is necessary for aquatic plants to photosynthesize. For this reason, treating textile wastewater properly is crucial to safeguarding the ecosystem and the surrounding environment [3].

To date, numerous techniques have been suggested to eliminate dyes from wastewater. For instance, some of the most widely utilised techniques include chemical precipitation, electrochemical oxidation, photochemical processes, ozonation, ion exchange, and chemical and Fenton processes [4]. Adsorption stands out among all of these techniques since it is affordable, environmentally benign, produces less sludge, and has no hazardous consequences. In adsorption, the adsorbent's surface is covered with the adsorbate that will help to remove dye ions from water or aqueous solution. Many diverse adsorbents are used for dye removal, such as nickel oxide [5], alumina [6], Hematite [7], Calcined products of Mg–Al layered double hydroxides/single-walled carbon nanotubes [8] etc. The remarkable effectiveness of oxides in eliminating organic contaminants from wastewater has been consistently demonstrated. Iron oxides, one of the most prevalent mineral groups on Earth, are among them and have shown to be helpful in a wide range of applications in both study and industry. Many people believe that these environmentally benign materials have a lot of potential for usage in a range of applications, particularly in magnetization, medical science, catalysis and environmental applications. Due to their superior adsorption affinity and capacity, quicker adsorption rate, and bigger surface areas when compared to other adsorbents they have interestingly shown tremendous promise as adsorbents for the removal of environment contamination [9].

Iron oxides' structural and textural characteristics, as well as their precursors and precipitation agents, have a substantial impact on their activity. There has already been a significant amount of published research on the adsorption of organic molecules into the synthetic iron oxides. For instance, sarker et al. (Sarker and Fakhruddin, 2017) produced rice straw and investigated the possibility of dye adsorption on it. Hematite (-Fe_2O_3), which effectively eliminates o-phthalic acid under a variety of environmental conditions, was created by Hwang et al [10]. Presently, iron oxide and the derivatives of iron oxide with another adsorbent are extensively used for dye removal of water from wastewater. Iron oxide is cheap and easily accessible and also has a high affinity than any other metal oxides. The surface area will increase with electrical, magnetic, and chemical properties during the elimination of dye due to its nanoscale structure and size. The high cost of activated carbon and regeneration losses prompted a search for less expensive bio-adsorbent [11]. In India, it is simple and common to obtain rice husk ash (RH). India is the second-largest producer of rice worldwide. Moreover, RH is waste from the manufacture of rice, which is used as cow feed and is likewise regarded as an efficient adsorbent [12]. Thorough literature search was done and to the best of our knowledge, no publications have been made about the RH+Fe used to remove dye from wastewater. This study synthesised RH+Fe, and then used a scanning electron microscope (SEM), X-ray powder diffraction (XRD), Fourier-transform infrared spectroscopy (FTIR), and particle size analysis to thoroughly analyse its physicochemical qualities as an adsorbent. Several parameter tests looked at the effects of time, adsorbent dose, pH, and beginning concentration. Kinetic, thermodynamic, and isotherm studies were used to demonstrate the dyeic property of the RH+Fe adsorbent. The potential of an adsorbent was also discovered through the study of regeneration research.

II. MATERIALS AND METHODS

A. *Materials*

Ferrous chloride ($FeCl_2.4H_2O$, 98%), Ferric chloride ($FeCl_3.6H_2O$, 98%), sodium hydroxide (NaOH, AR 99%), and dye (A.R. 98%) were procured from Merck. Rice husk was purchased from nearby rice mill. All of the substances were highly pure analytical reagents that were employed in the studies. Demineralized water was utilised for chemical preparations and testing in later research.

B. *Preparation of RH adsorbent*

RH was washed with 10 % HCL and kept in the oven for drying at 90 ºC for 20 h. After that RH was crushed and kept at 500 ºC in a muffel furnace for 8 h and form a white color powder. RH was sieved through 425 µm and washed five times with demineralized water and dried again in the oven at 60 ºC for 24 h.

C. *RH+Fe oxide Synthesis*

For RH+Fe NPs synthesis, co-precipitation technique was used. The NPs was synthesized using Ferric chloride (4 g), Ferrous chloride (4g) and RH (8 g) with HCL dissolved in demineralized water (200 mL) in a beaker at 90 ºC for 120 min for 8 h. The dropwise 1.5 M NaOH was added while stirring. Then the NPs was centrifuged at 2500 rpm for 20 min and separated in filter paper. Afterwards, the filter paper was kept in oven for 4 h at 90 ºC. Lastly, the powdered RH+Fe was obtained and stored in a small bottle.

D. *Batch Adsorption Experiments*

In this study, RH+Fe nanoparticles (NPs) adsorbent was employed in batch studies to optimise the parameters while dye was assessed utilising the dye assay process. Each experiment was carried out in a beaker containing 100 mL of dye solution, and the required NPs quantities were agitated in an orbital shaker. Before filtering it via Whatman filter paper, the solution was agitated. Later, the filtered solution was evaluated using the APHA 23rd edition dye assay technique. NaOH (0.1 M) and HCL (0.1 M) were employed in tests to modify the pH solution. Using equations (1) and (2), the effectiveness of dye removal and adsorption capacity were assessed.

$$\%\text{Removalefficiency} = \frac{C_i - C_e}{C_i} \times 100 \quad (1)$$

$$q_e = \frac{(C_O - C_e)V}{m} \quad (2)$$

Whereas C_i and C_e represent initial and equilibrium concentrations of dye in solution (g L^{-1}), V is the volume of the solution (L), and m is the mass of the adsorbent (g).

E. Characterization of RH+Fe adsorbent

For characterization, by using the KBr pellet method and FTIR spectroscopy (Nicolet 6700), the types of bonds present in the adsorbent were identified in the 400–4000 cm^{-1} range. An X-ray diffractometer (PAN analytical X'pert PRO) investigation uses Cu-K radiation (1.5406 Å) at an accelerating voltage of 40 kV and a current of 30 mA to identify the phases of the NPs. The morphology of the particle was subsequently determined using TEM on a JEM 2100 (Make: JEOL) microscope. Field Emission-Scanning Electron Microscope (FE-SEM) (Zeiss Ultra 55) was used to examine the adsorbent's morphology, size, and structure. The material was mixed in the solvent also coated with gold for examination. A Malvern 890 particle size analyzer made it possible to determine the NPs size.

III. RESULTS AND DISCUSSION

Later, to evaluate the amount of dye removed from RH+Fe after and before adsorption (AD & BD), FTIR was used, as shown in Fig. 2. RH+Fe research on BD and AD shows no distinctions between the two. The pure Fe spectrum, which is present at 557 cm-1, is due to vibrations peculiar to the Fe-O bond. SiO2 was discovered at 879 cm-1. The peaks at 1627 cm-1, 1429 cm-1, and 2360 cm-1 additionally indicate the O-H, CH3, C=C, and C-H bonds. Assignments for frequency and position were shown in Table 1 [13].

Further, the characteristic diffraction peak in RH+Fe AD and BD was identified using an X-ray diffractometer, as shown in Fig. 3. The peaks were attributed to the Joint Committee on Powder Diffraction Standards (JCPDS) X-ray data file. Patterns of RH+Fe were 22.0°, 25.2°, 27.1°, 30.0°, 32.1°, 38.4°, 44.2°, 57.2°, and 63.0° at its peak value of 2Θ, which corresponds to the peak (004), (420), (151), (220), (600), (311,040), (222), (110), (422), (511), and (440). While the peak of Fe-O was apparent at 30.0°, the peak of SiO_2 is seen in the conspicuous peaks at 35.4°. The prominent peak of the adsorbent indicates the crystalline nature of the materials. Using the Debye-Scherer equation, it was found that the average crystallite size of these NPs was 55.7 nm, where h is the Bragg angle, K is the Debye-Scherer constant (0.9), β is the full width at half maximum of the biggest peak, and is the X-ray wavelength close to 1.5406 Å (in radians). As a result, the XRD results confirmed that RH+Fe was produced by synthesis process [14].

Later on, in Fig 4 the SEM analysis shows the flower-type image of indicate the adsorption of RH in Fe. The colloidal formation indicates the Fe NPs was prepared. Magnetic property helps the iron oxide NPs to attract dye which helps in removal of aqueous solution. While EDX analysis was confirmed the elemental composition showing 48 % of iron, 23 % of RH and 29 % of oxygen which is an indication for successful formation of material [15].

For RH+Fe NPs, The particle dispersion was determined using a particle size analyzer, as shown in Fig. 5. The average size of the adsorbent is 78 nm. The conjoining of NP makes the size of the adsorbent important [16].

A. Different parameters analysis

1) Effect of Dosage, contact time, concentration, and pH

At a constant temperature of 50° C and 200 rpm of stirring, batch investigations of adsorbent dosage for RH+Fe adsorbent for defluoridation were carried out. It was clear from Fig. 6 that the removal efficiency of the Dye trend line rose from 0.1 to 3 g L^{-1} but remained constant at 2.6 g L^{-1}. The availability of a broad surface area and additional adsorption sites with increasing adsorbent dosage causes the removal efficiency to increase. Due to the overlapping of active sites at higher dosages and the absence of holes in the adsorbent's active surface area, the adsorption remains constant. The process of surface adsorption depended heavily on the volume of micropores and the accessibility of a definite surface area. On RH+Fe adsorbent, the highest Dye adsorption was 98 % at 88 mg g^{-1} adsorption capacity [17].

In a batch experiment, the Dye removal effectiveness was demonstrated by maintaining a dose of 2.6 g L^{-1} at a temperature of 50° C and stirring at a velocity of 200 rpm, as shown in Fig. 7. When the RH+Fe was utilized for Dye adsorption, the removal effectiveness of the Dye increased up to 60 min, reaching 98 %, and then remained steady until 90 min, where adsorption capacity reaches to 88 mg g^{-1}. This trend can be caused by the porous structure's maximal active sites for adsorption with the passage of time and the surface area's high surface area. Additionally, as time passes, the adsorption stays constant since an oxidant is no longer available for adsorption. Two crucial mechanisms contributed to the decline in Dye adsorption; one was the diffusion phenomenon which occurs among the pores and active surface area in the adsorbent. Another argument was made when the Dyeate ions were adsorbed on the surface sites, and the repulsion was produced between Dye and the adsorbent [18].

The concentration was examined with constants such as a dosage of 2.6 g L^{-1}, temperature 50 °C, stirring rate 200 rpm, and time 60 min for the RH+Fe adsorbent in a batch experiment between 10 mg L^{-1} and 100 mg L^{-1} shown in Fig. 8.

The elimination of Dye increases significantly in 10 mg L^{-1} with 98 % removal efficiency and 88 mg g^{-1} adsorbent capacity, according to the study. Due to additional binding sites being available at a lower concentration, the initial concentration then rises. Due to active sites saturation, reduced mass transfer, and a shortage of binding sites for Dye adsorption, adsorption reduces at increasing concentrations. Later, the experimental Dye adsorption data were identified and presented below using isotherms and kinetic model [19].

The pH of an aqueous solution is the most important element in determining how ions are adopted on the surface of an oxide. In experiments conducted in the pH range of 2-12 with a dose of 2.6 g L^{-1} at a temperature of 50 °C, stirring rate of 200 rpm, and a duration of 60 min, the interaction of the Dyeate ion and the RH+Fe was focused on pH. The adsorption capacity of Dye was shown to increase with initial pH value and gradually decline with higher pH. This cause under the interfacial attraction on the adsorption properties of dye. The higher pH is at 6 due to the strong π- π interaction and H-bond interaction between the adsorbent and dye. At higher pH the decrement in adsorption is due to homogenous charge repulsion between the dyeates and negatively charge RH+Fe. As a result, for the RH+FeNPs, the maximum adsorption capacity was attained 98 % removal efficiency at 6 pH and 88 mg g^{-1} adsorbent capacity as shown in Fig 9 [20].

2) Adsorption Kinetics

The experimental data were fitted to kinetic models such as the pseudo-first order, and pseudo-second order was followed to better describe the potential adsorption, mechanism of Dye on the adsorbent, and the correlative parameters. The eq. (6 & 7) are displayed below.

$$\log(q_e - q_t) = \log q_e - \frac{k_1 t}{2.303} \quad (6)$$

$$\frac{t}{q_t} = \frac{1}{k_2 q_e^2} + \frac{t}{q_e} \quad (7)$$

The fitted kinetic model is shown in Fig. 10, and all the data are shown in Table 2. The eq. (6). is pseudo first order where qe and qt denote the amount of Dye adsorbed (mg g^{-1}) at equilibrium and at time t, respectively. K_f (min^{-1}) is the rate constant of pseudo-first-order adsorption reaction. The eq.(7) shows pseudo-second- order reaction where Ks is the rate constant for the pseudo-second- order reaction (g mg^{-1} min^{-1}). q_e and q_t are the amounts of solute adsorbed at equilibrium and at any time t (mg g^{-1}) [21].

The correlation coefficient R^2 was discovered to be the most significant and been made best match by experimental data. Among these two pseudo-second order (R^2 = 0.97), provided the best explanation for the kinetic data. Thus, chemical interactions i.e., chemisorption phenomena relating valency forces through sharing or exchange of electrons between sorbent and sorbate, were the rate-limiting step (Liu et al., 2010). The standard deviation (sd) was used to evaluate the kinetic models that were used to match the sorption data. In Pseudo first order model, smaller sd values show that Dye adsorption is dependent on the active sites on RH+Fe composite.

3) Adsorption Isotherms

The feasibility of the reaction, the interface between the Dye and RH+Fe adsorbent, the adsorption characteristics, the peripheral phenomena of the NPs, and the equilibrium data were all examined using isotherms. The investigational data from Langmuir and Freundlich were examined in this work along with varying beginning concentrations (10-100 mg L^{-1}) with 2.6 g L^{-1} dosage of RH+Fe adsorbent, as shown in Table 3 and Fig. 11.

The Langmuir isotherm presupposes either monolayer adsorption or uniform dispersion of the adsorbent with a restricted number of identical sites on homogeneous surfaces. For the RH+Fe adsorbent had an adsorption capacity of 90 mg g^{-1}, and the graph was plotted with Ce/qe and qe and R^2 0.96 [22].

$$\frac{C_e}{Q_e} = \frac{1}{q_m b} + \frac{C_e}{q_m} \quad (8)$$

The equation was stated in eq. (8) where, Q_e is the equilibrium amount of adsorbate in adsorbent (mg g^{-1}), C_e is the equilibrium concentration capacity (mg L^{-1}), q_m is the maximum Dye adsorption capacity (mg g^{-1}), and b is the isotherm constant (mg L^{-1}).

When it comes to multilayer adsorption in the Freundlich isotherm, the non-ideal and reversible adsorption is characterised by heterogeneous surfaces and an uneven distribution of adsorption sites. The graph, of log Q_e and log C_e was plotted, shows Dye adsorption on RH+Fe in Fig. 11b and provides values of K_f and 1/n with R^2 0.95 [23].

$$\log Q_e = \log K_f + \frac{1}{n}\log C_e \quad (9)$$

The equation was stated in eq. (9), where K_f = Freundlich equilibrium constant (L g^{-1}), and 1/n = constant related to energy of adsorption intensity in a heterogeneous system.

The experimental and estimated value were resolute, together with R^2, to assess best-fitting isotherm. Table 3 displays the R^2 value. In comparison to Langmuir and Freundlich, Langmuir have a higher R^2 value. Due to the establishment of an ionic and covalent link between Dye and RH+Fe, monolayer adsorption and homogenous surface will be implied according to Langmuir theory. Additionally, the Freundlich isotherms fall between 1 and 10, indicating that the Dye was readily adsorbed on the adsorbent's surface. Table 4 compares several adsorbents based on their capacity for adsorption.

4) Thermodynamics Study

The results of the investigation into how temperature affects the dye's adsorption to the RH+Fe are displayed in Fig. 12. The temperature optimisation and plot of T^{-1} vs. lnK were shown in Fig. 12(a) & (b). The adsorption process and its possibilities were examined in the thermodynamic process. Using Fig. (12b), the standard enthalpy (ΔH^o) and standard entropy (ΔS^o) change, as well as the intercept and slope, were calculated. The difference in Gibbs free energy (ΔG^o) was calculated using eq. (10–12). The outcome is displayed in Table 5. The dye adsorption rises with temperature. The adsorption has a more significant cause, which is why the reaction adheres to the La Chattelier principle. The value of (ΔG^o) increases as the temperature increases. This proves that the adsorption occurred on its own. The increased randomness at the solid-liquid interface is shown to increase as the number of species increases by the positive value of the (ΔS^o). When dye and a solid surface come into touch, water molecules are released. The (ΔH^o) value denotes the type of physical adsorption that is occurring in the system, which is surface adsorption of RH+Fe. By a positive (ΔH^o) result, the endothermic adsorption is verified [24]. As a result, in the present investigation, higher temperatures were preferred than lower temperature.

$$\Delta G^\circ = RT\ \ln K_C \quad (10)$$

$$\Delta G^\circ = \Delta H^\circ - T\Delta S^\circ \quad (11)$$

$$\log\left(\frac{q_e m}{C_e}\right) = \frac{\Delta S^\circ}{2.303R} + \frac{-\Delta H^\circ}{2.303RT} \quad (12)$$

Where R= universal gas constant (8.314 J mol^{-1} K^{-1}), and Kc = adsorption distribution coefficient.

5) Recyclability Study

Reusability is a key factor to take into account when considering whether to employ an adsorbent practically for commercial reasons. The investigation was conducted using batch experiments, and the graph is shown in Fig. 13. Following that, 0.1 M NaOH was used to stir the used adsorbent solution for 2 h. After centrifuging, the adsorbent was baked for 8 h at 90º C. Aiming all stages, recycled adsorbent was applied once more under identical conditions with a starting concentration of 10 mg L^{-1}. The fifth cycle, which is depicted in Fig. 13, produced dye with an efficiency of 56 %. Efficiency declines as a result of patches on the adsorbent's surface becoming inaccessible. The results showed that the adsorbent that had been treated with NaOH could regenerate and be reused quickly, proving that the material was effective, affordable, and environmentally friendly with amazing reusability and its true application potential [25].

IV. CONCLUSIONS

The RH+Fe adsorbent was used in the current work to achieve dye efficiency. The characterisation demonstrates that the RH+Fe adsorbent was expertly made. The ideal parameters were concentration10 mg L^{-1}, dosage 2.6 g L^{-1}, pH 6, and time 60 min, with a 98 % dye elimination efficiency. The adsorption of dye and RH+Fe was largely dependent on optimised parameters. The RH+Fe adsorbent data was best suited to the Langmuir isotherm and had an adsorption capacity of 98 mg g^{-1}, which is monolayer adsorption between adsorbate and adsorbent, according to calculations made from the equilibrium data. The regeneration of dye elimination indicated 56 % in the fifth stage. As a result, this study significantly advances our knowledge of viable and useful methods for removing dye from adsorbents.

REFERENCES

[1] Chang JS, Chen BY, Lin YS. Stimulation of bacterial decolorization of an azo dye by extracellular metabolites from Escherichia coli strain NO3. Bioresour Technol 2004;91:243–8. https://doi.org/10.1016/S0960-8524(03)00196-2.
[2] Eren E. Investigation of a basic dye removal from aqueous solution onto chemically modified Unye bentonite. J Hazard Mater 2009;166:88–93. https://doi.org/10.1016/j.jhazmat.2008.11.011.
[3] Moussavi G, Mahmoudi M. Removal of azo and anthraquinone reactive dyes from industrial wastewaters using MgO nanoparticles. J Hazard Mater 2009;168:806–12. https://doi.org/10.1016/j.jhazmat.2009.02.097.
[4] Mandal A, Mukhopadhyay P, Das SK. The study of adsorption efficiency of rice husk ash for removal of phenol from wastewater with low initial phenol concentration. SN Appl Sci 2019;1:1–13. https://doi.org/10.1007/s42452-019-0203-3.
[5] Dehmani Y, Alrashdi AA, Lgaz H, Lamhasni T, Abouarnadasse S, Chung IM. Removal of phenol from aqueous solution by adsorption onto hematite (α-Fe2O3): Mechanism exploration from both experimental and theoretical studies. Arab J Chem 2020;13:5474–86. https://doi.org/10.1016/j.arabjc.2020.03.026.
[6] Li S, Qin GW, Zhang Y, Pei W, Zuo L, Esling C. Anisotropic growth of iron oxyhydroxide nanorods and their photocatalytic activity. Adv Eng Mater 2010;12:1082–5. https://doi.org/10.1002/adem.201000081.
[7] Lassoued A, Dkhil B, Gadri A, Ammar S. Control of the shape and size of iron oxide (α-Fe2O3) nanoparticles synthesized through the chemical precipitation method. Results Phys 2017;7:3007–15. https://doi.org/10.1016/j.rinp.2017.07.066.
[8] Ahmad A, Mohd-Setapar SH, Chuong CS, Khatoon A, Wani WA, Kumar R, et al. Recent advances in new generation dye removal technologies: Novel search for approaches to reprocess wastewater. RSC Adv 2015;5:30801–18. https://doi.org/10.1039/c4ra16959j.
[9] Kong LP, Gan XJ, Ahmad AL bin, Hamed BH, Evarts ER, Ooi BS, et al. Design and synthesis of magnetic nanoparticles augmented microcapsule with catalytic and magnetic bifunctionalities for dye removal. Chem Eng J 2012;197:350–8. https://doi.org/10.1016/j.cej.2012.05.019.
[10] Hwang YS, Liu J, Lenhart JJ, Hadad CM. Surface complexes of phthalic acid at the hematite/water interface. J Colloid Interface Sci 2007;307:124–34. https://doi.org/10.1016/j.jcis.2006.11.020.
[11] Rizzi V, Longo A, Fini P, Semeraro P, Cosma P, Franco E, et al. Applicative Study (Part I): The Excellent Conditions to Remove in Batch Direct Textile Dyes (Direct Red, Direct Blue and Direct Yellow) from Aqueous Solutions by Adsorption Processes on Low-Cost Chitosan Films under Different
[12] He D, Ikeda-Ohno A, Boland DD, Waite TD. Synthesis and characterization of antibacterial silver nanoparticle- impregnated rice husks and rice husk ash. Environ Sci Technol 2013;47:5276–84. https://doi.org/10.1021/es303890y.
[13] Swarnav M. Preparation and Characterization of Cu-Cr Impregnated Silica Catalyst from Rice Husk 2014.
[14] Gupta A, Balomajumder C. Simultaneous Adsorption of Cr(VI) and Phenol from Binary Mixture Using Iron Incorporated Rice Husk: Insight to Multicomponent Equilibrium Isotherm. Int J Chem Eng 2016;2016:1–11. https://doi.org/10.1155/2016/7086761.
[15] Hoyos-Sánchez MC, Córdoba-Pacheco AC, Rodríguez-Herrera LF, Uribe-Kaffure R. Removal of Cd (II) from Aqueous Media by Adsorption onto Chemically and Thermally Treated Rice Husk. J Chem 2017;2017:1–8. https://doi.org/10.1155/2017/5763832.
[16] Srivastava VC, Mall ID, Mishra IM. Optimization of parameters for adsorption of metal ions onto rice husk ash using Taguchi's experimental design methodology. Chem Eng J 2008;140:136–44. https://doi.org/10.1016/j.cej.2007.09.030.
[17] Gebrewold BD, Kijjanapanich P, Rene ER, Lens PNL, Annachhatre AP. Fluoride removal from groundwater using chemically modified rice husk and corn cob activated carbon. Environ Technol (United Kingdom) 2018;0:1–15. https://doi.org/10.1080/09593330.2018.1459871.
[18] Pillai P, Lakhtaria Y, Dharaskar S, Khalid M. Synthesis, characterization, and application of iron oxyhydroxide coated with rice husk for fluoride removal from aqueous media. Environ Sci Pollut Res 2020;27:20606–20. https://doi.org/10.1007/s11356-019-05948-8.
[19] Hassan AF, Abdelghny AM, Elhadidy H, Youssef AM. Synthesis and characterization of high surface area nanosilica from rice husk ash by surfactant-free sol-gel method. J Sol-Gel Sci Technol 2014;69:465–72. https://doi.org/10.1007/s10971-013-3245-9.
[20] Kadhim A-SF. Characterization the Removal of Phenol from Aqueous Solution in Fluidized Bed Column by Rice Husk Adsorbent. Res J Recent Sci 2012;1:145.
[21] Chandrasekhar S, Pramada PN. Rice husk ash as an adsorbent for methylene blue-effect of ashing temperature. Adsorption 2006;12:27–43. https://doi.org/10.1007/s10450-006-0136-1.
[22] Pillai P, Dharaskar S, Sinha MK, Sillanpää M, Khalid M. Iron oxide nanoparticles modified with ionic liquid as an efficient adsorbent for fluoride removal from groundwater. Environ Technol Innov 2020;19:100842. https://doi.org/10.1016/j.eti.2020.100842.
[23] Raul PK, Devi RR, Umlong IM, Banerjee S, Singh L, Purkait M. Removal of Fluoride from Water Using Iron Oxide-Hydroxide Nanoparticles. J Nanosci Nanotechnol 2012;12:3922–30. https://doi.org/10.1166/jnn.2012.5870.
[24] Predescu AM, Matei E, Berbecaru AC, Pantilimon C, Drăgan C, Vidu R, et al. Synthesis and characterization of dextran-coated iron oxide nanoparticles. R Soc Open Sci 2018;5. https://doi.org/10.1098/rsos.171525.
[25] Hao L, Liu M, Wang N, Li G. A critical review on arsenic removal from water using iron-based adsorbents. RSC Adv 2018;8:39545–60. https://doi.org/10.1039/c8ra08512a.

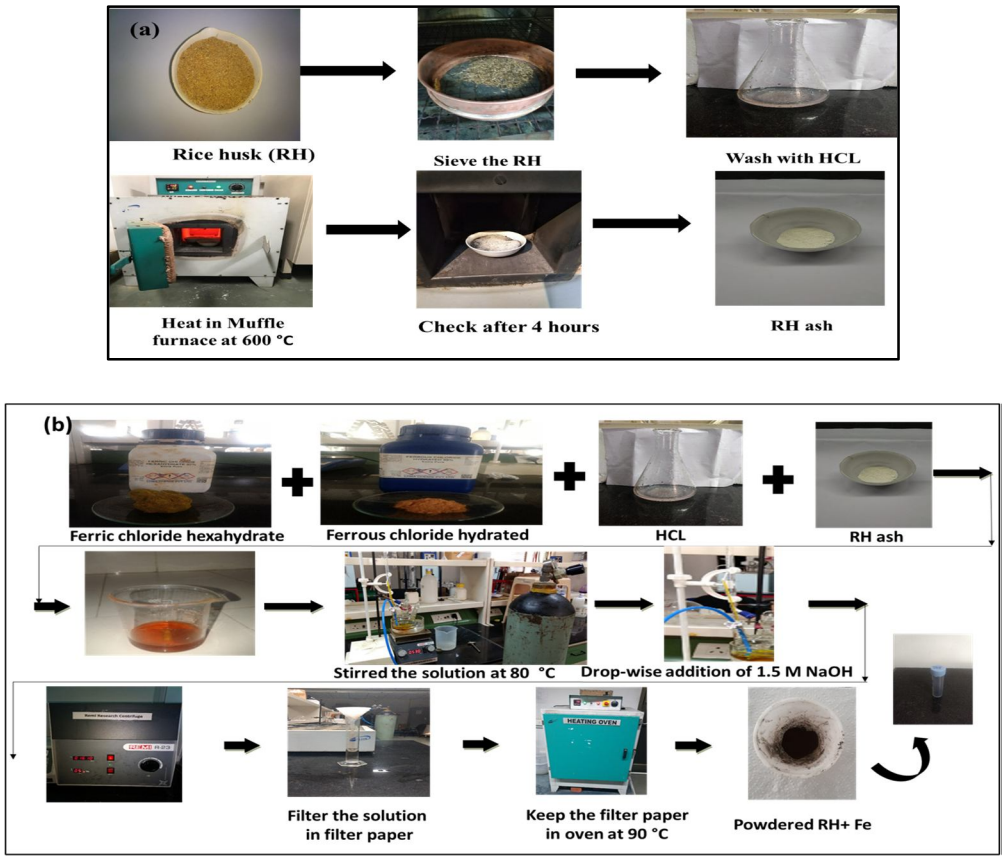

Fig 1. Synthesis process of adsorbent which were done in lab

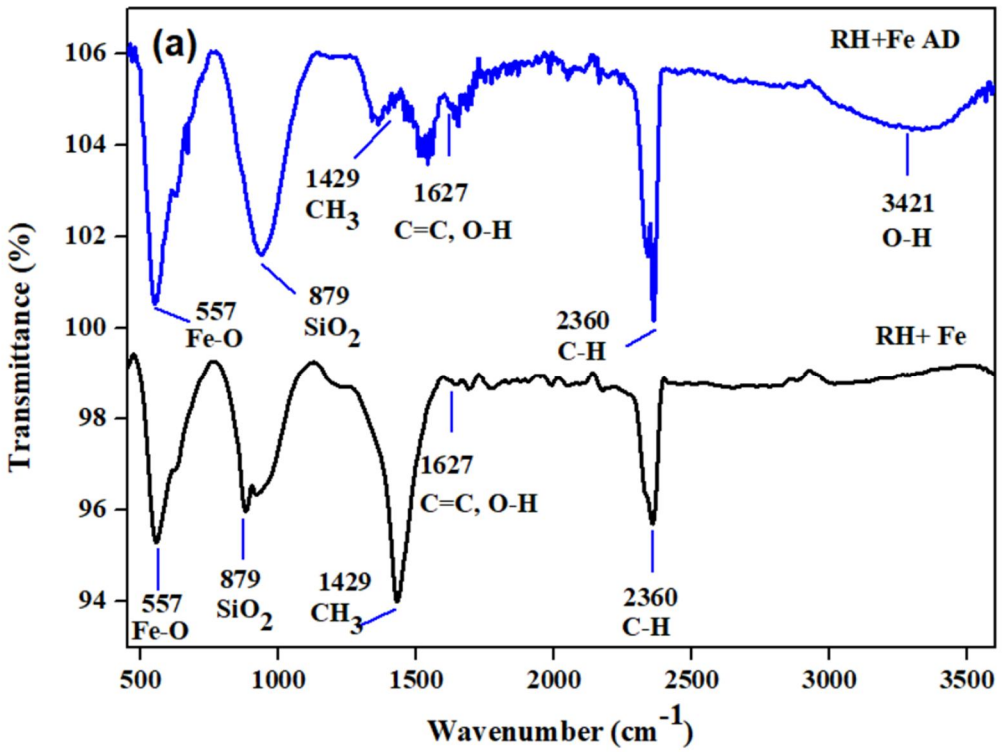

Fig 2. FTIR spectra of adsorbent

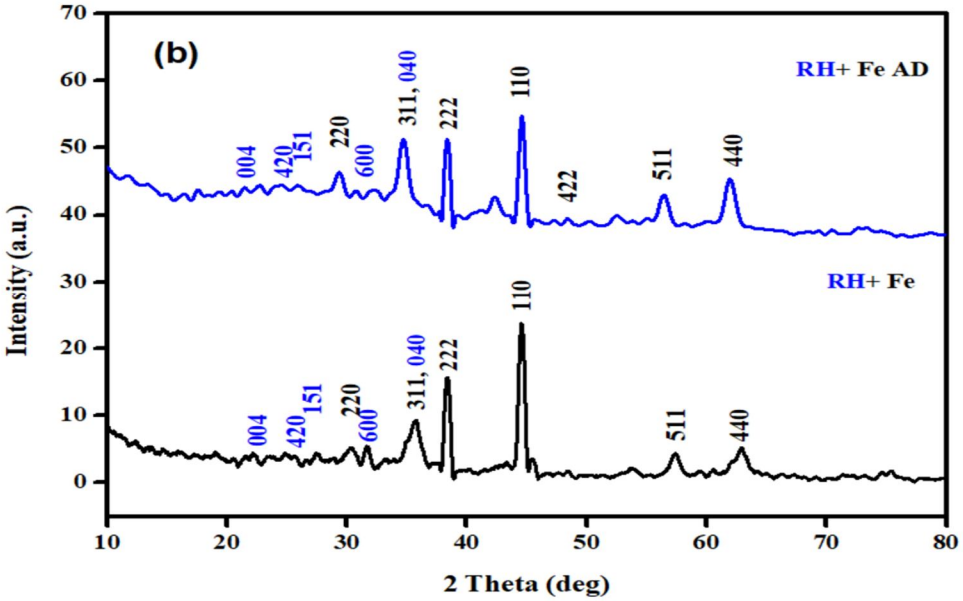

Fig 3. XRD of adsorbent

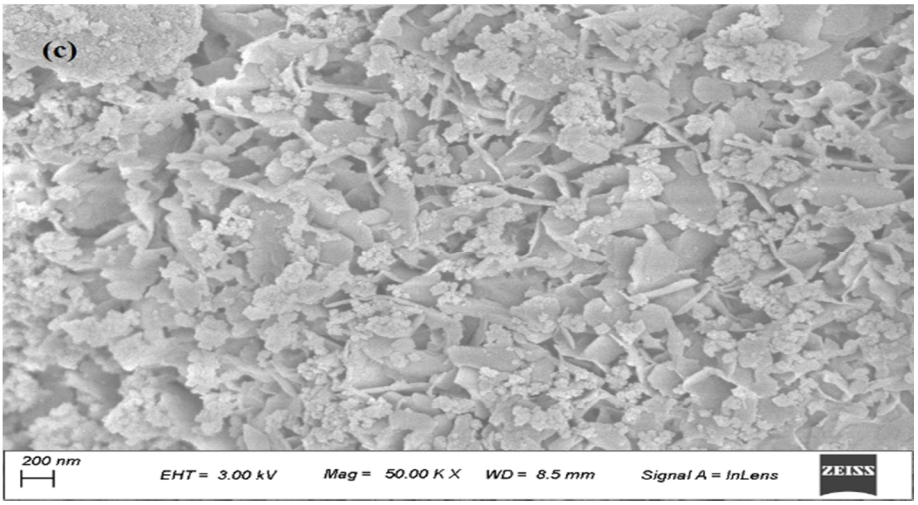

Fig 4. SEM of adsorbent

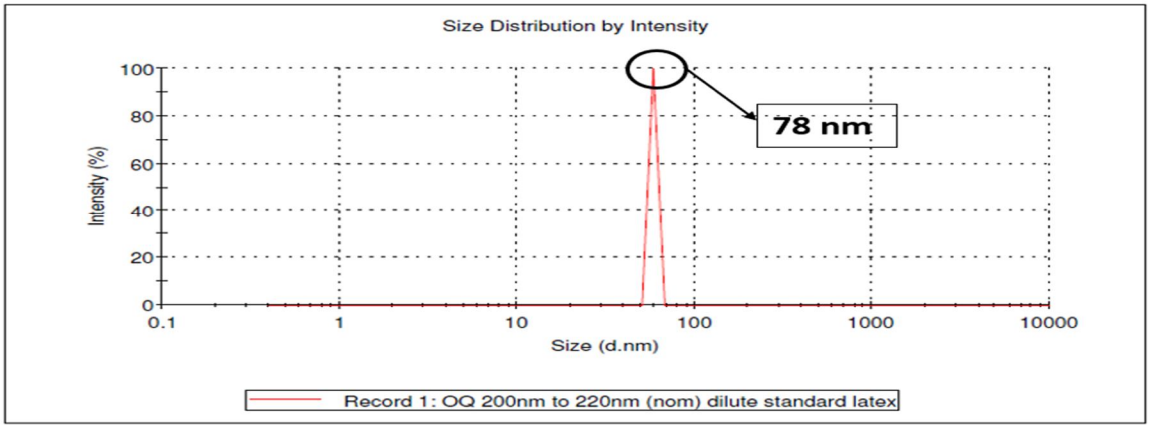

Fig 5. Particle size analysis of adsorbent

ISSN: 2321-9653; IC Value: 45.98; SJ Impact Factor: 7.538
Volume 13 Issue II Feb 2025- Available at www.ijraset.com

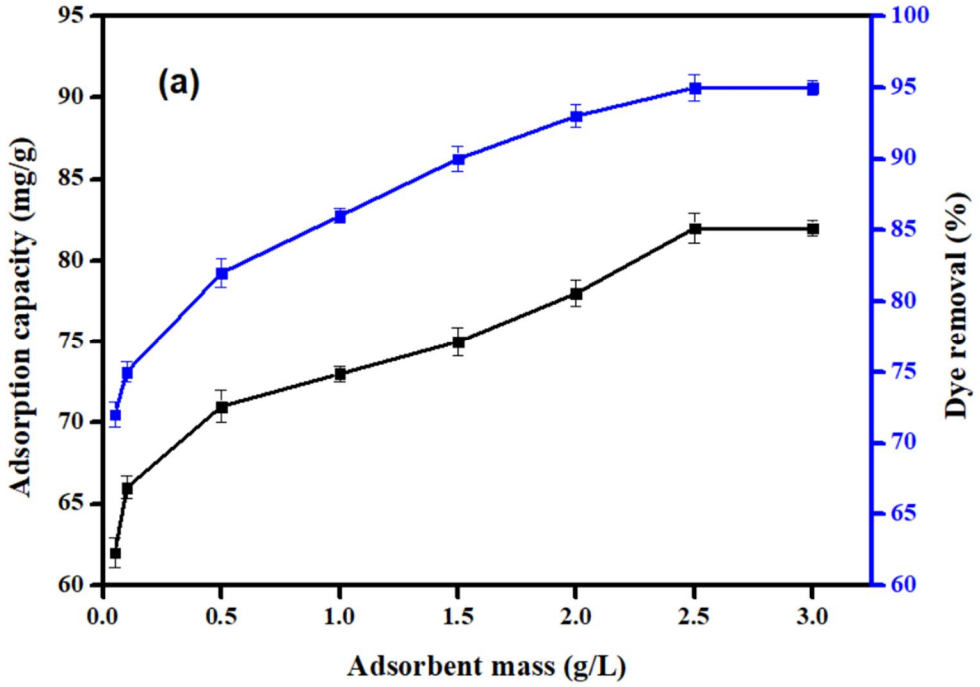

Fig 6. Effect of dosage of adsorbent (C_0: 10 mg/L, Contact time: 60 min, T: 50 ºC, Agitation speed: 200 rpm, pH: 6)

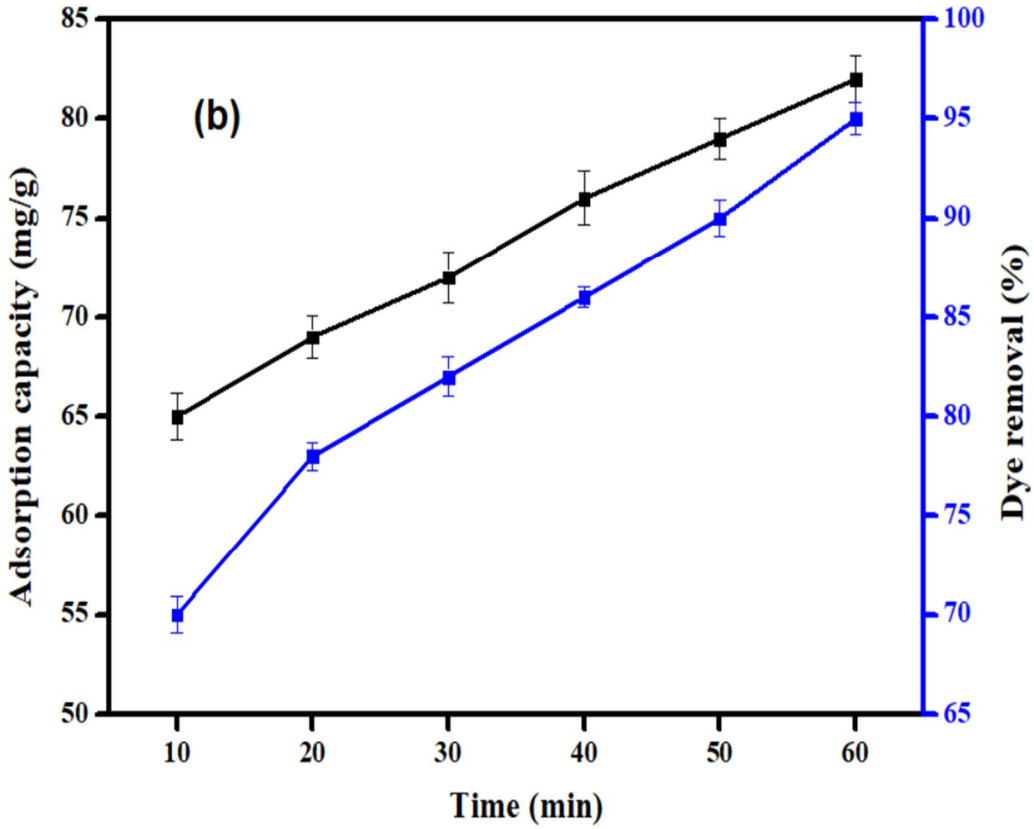

Fig 7. Effect of time of adsorbent (C_0: 10 mg/L, Adsorbent dosage: 2.5 g/L, T: 50 ºC, Agitation speed: 200 rpm, pH: 6)

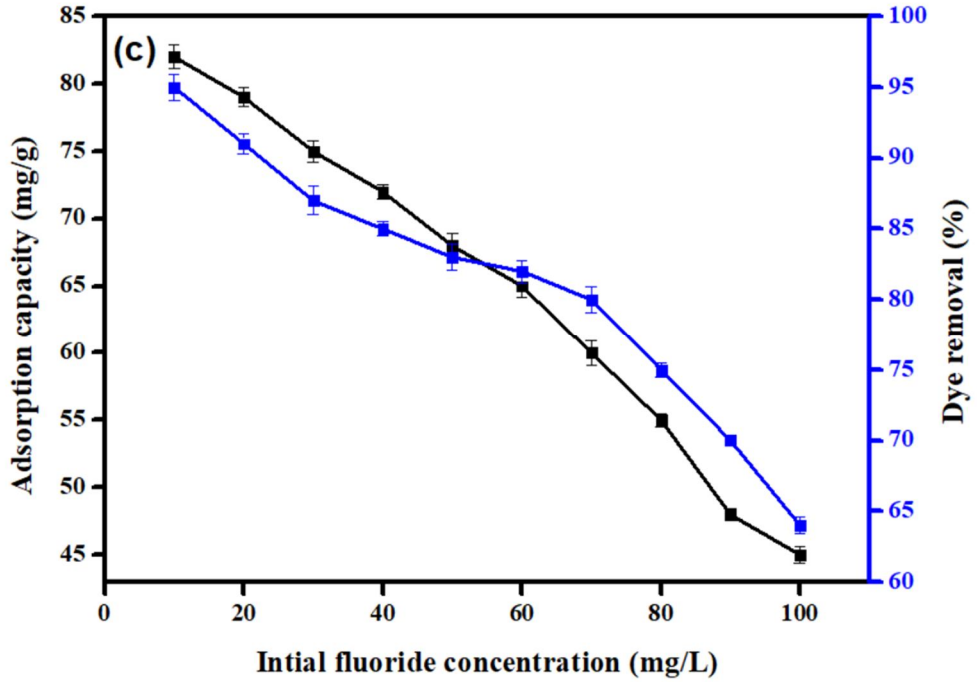

Fig 8. Effect of the initial concentration of adsorbent (Adsorbent dosage: 2.5 g/L, Contact time: 60 min, T: 50 ºC, Agitation speed: 200 rpm, pH: 6)

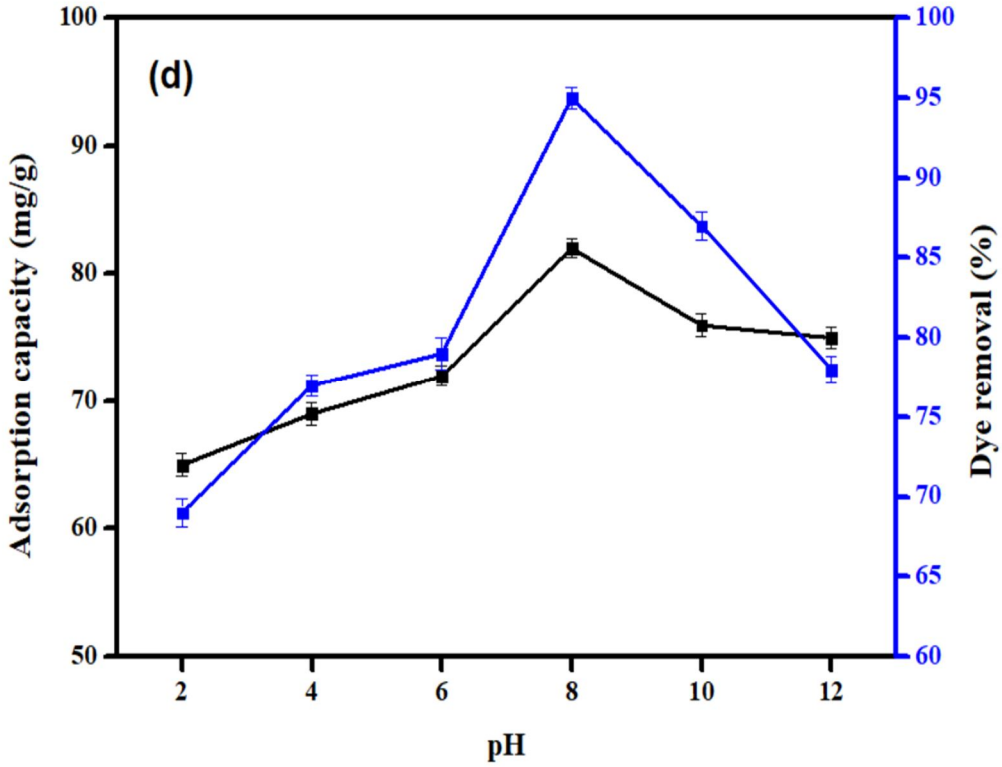

Fig 9. Effect of pH of adsorbent (Adsorbent dosage: 2.5 g/L, Contact time: 60 min, T: 50 ºC, Agitation speed: 200 rpm, C_0: 10 mg/L)

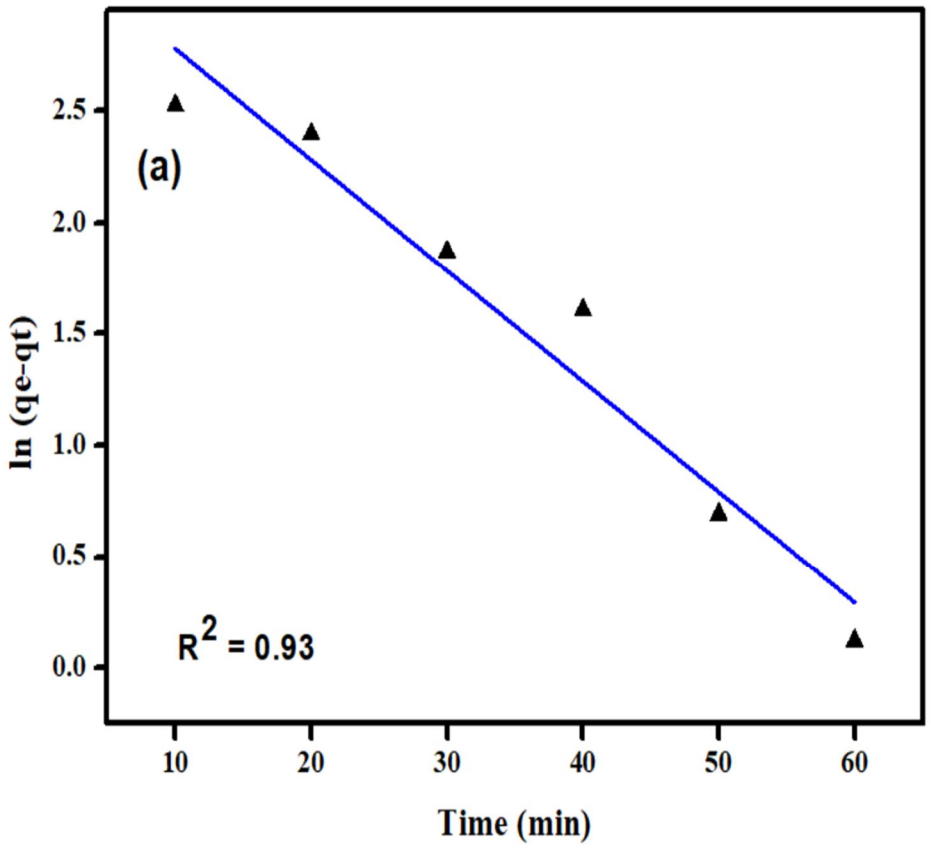

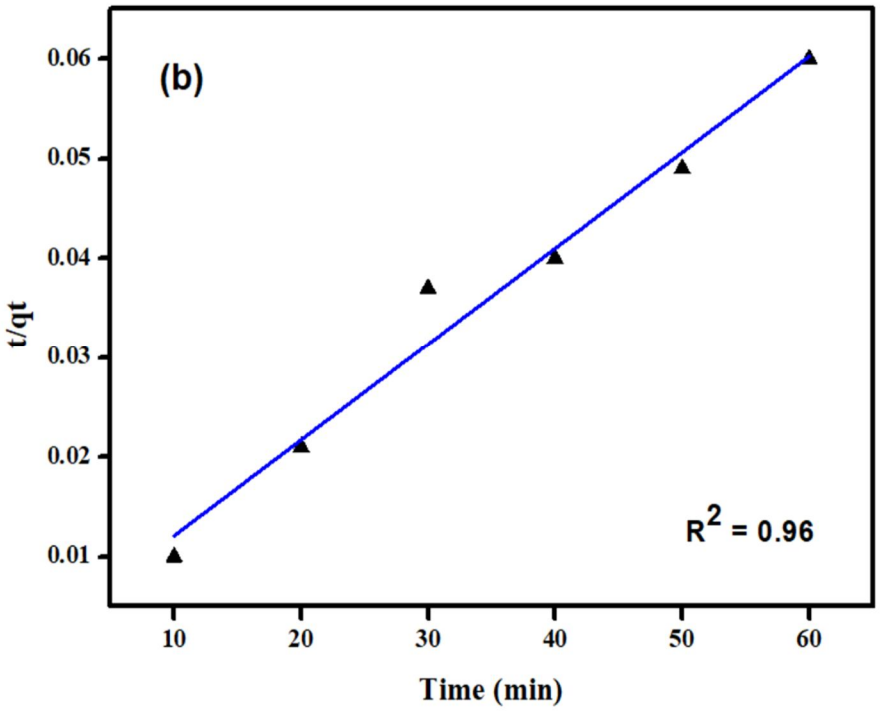

Fig 10. Kinetic study (a) pseudo-first-order (b) pseudo-second-order

ISSN: 2321-9653; IC Value: 45.98; SJ Impact Factor: 7.538
Volume 13 Issue II Feb 2025- Available at www.ijraset.com

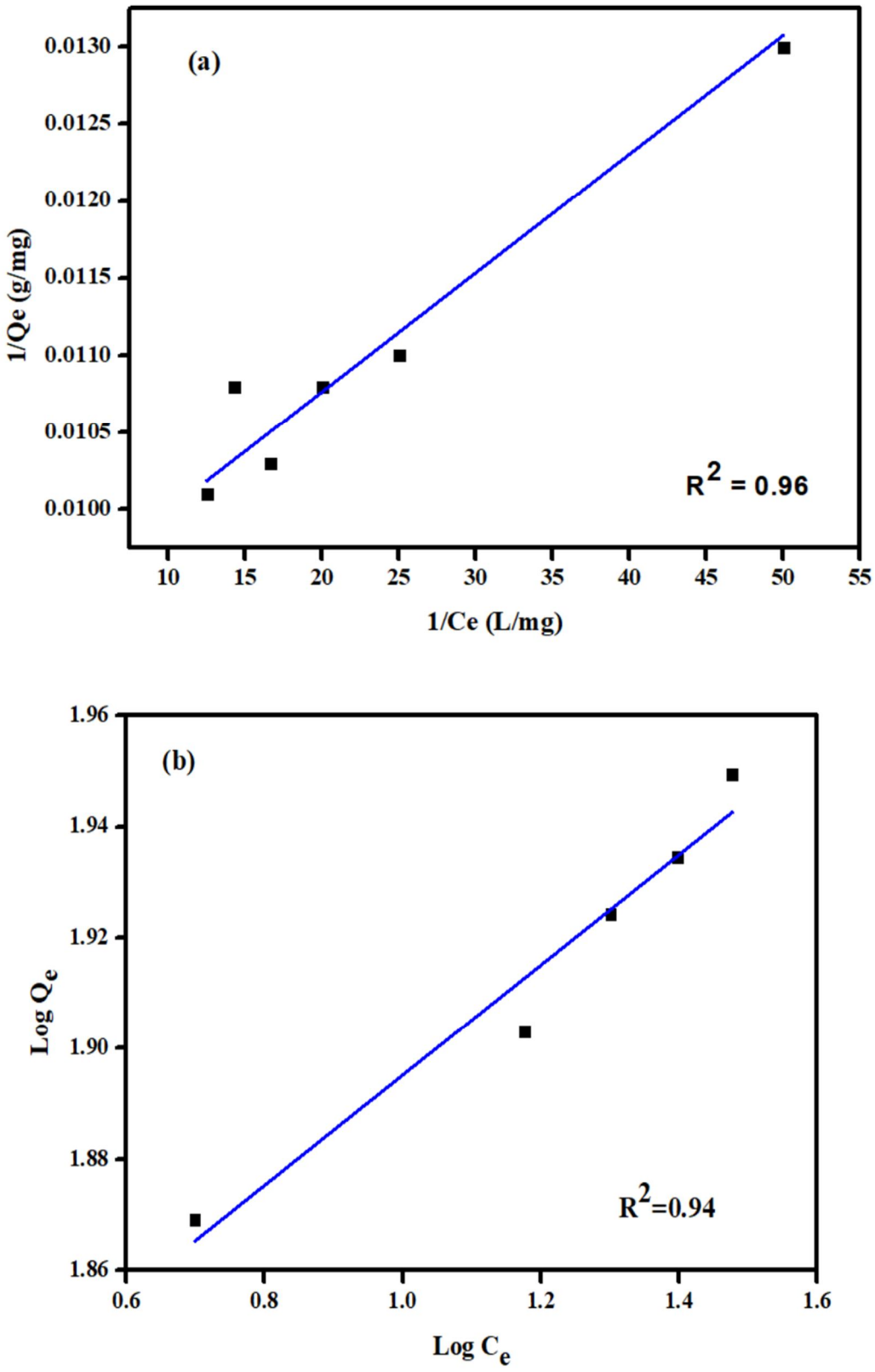

Fig 11. Isotherm study (a) Langmuir (b) Freundlich

ISSN: 2321-9653; IC Value: 45.98; SJ Impact Factor: 7.538
Volume 13 Issue II Feb 2025- Available at www.ijraset.com

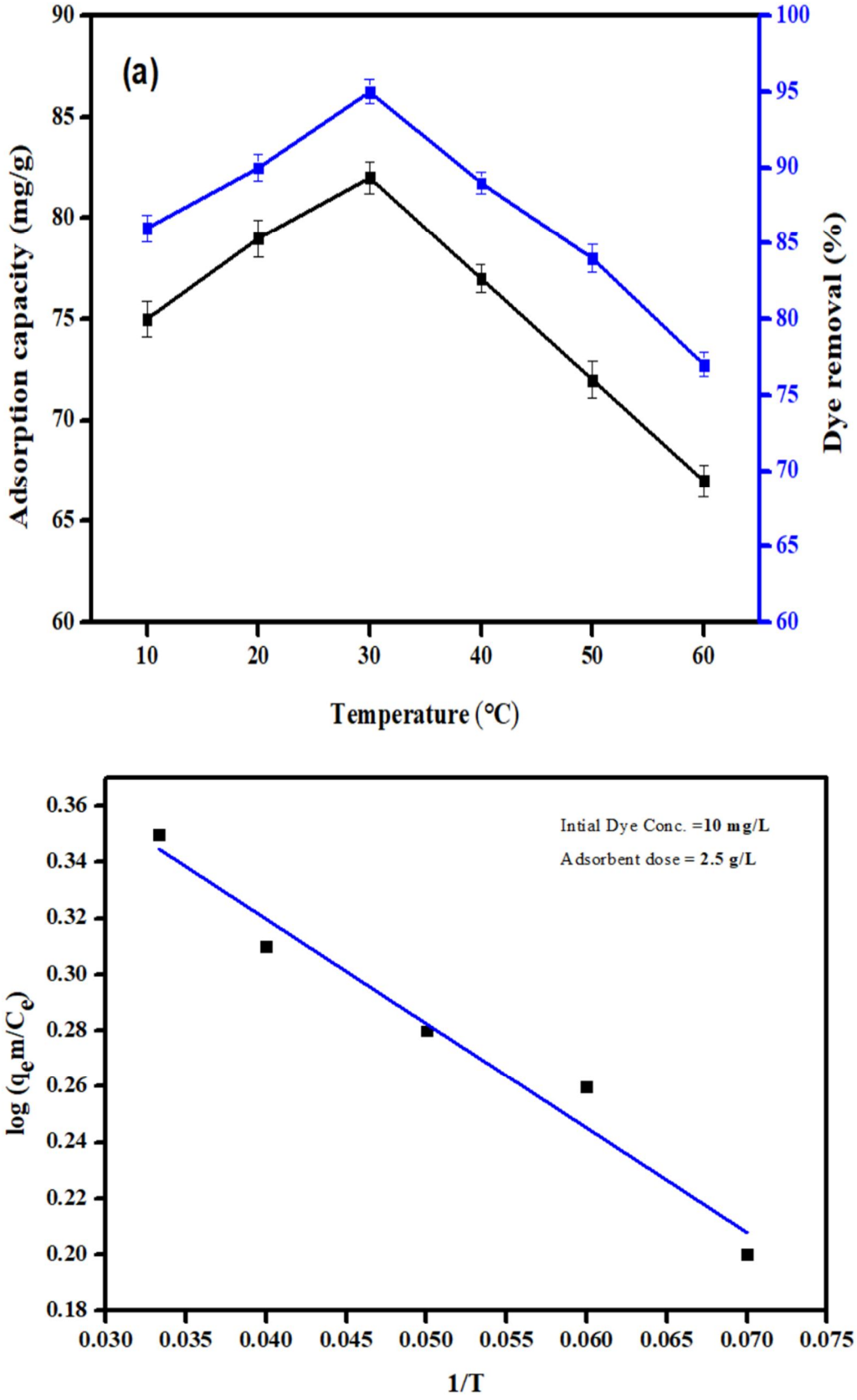

Fig 12. (a) Temperature study (b) Thermodynamic study

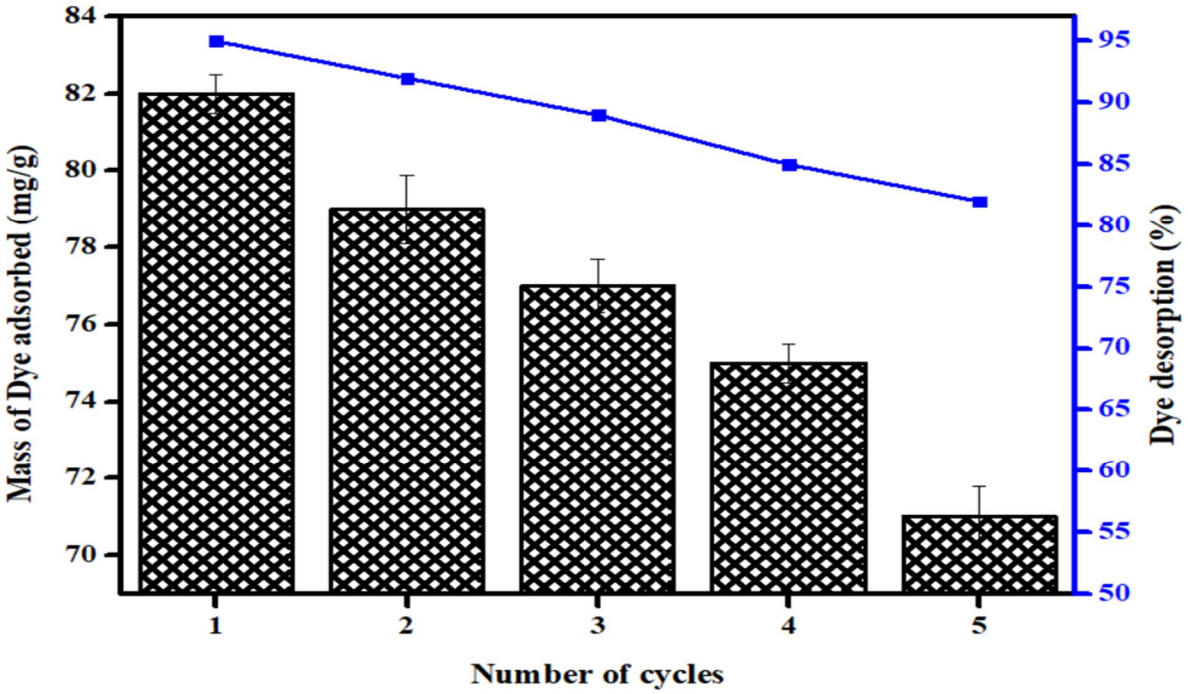

Fig 13. Regeneration study (Adsorbent dose: 2.5 g/L, Contact time: 60 min, T: 50 ºC, Agitation speed: 200 rpm, pH: 7)

Table 1. FTIR table for RH+Fe adsorbent.

Frequency cm^{-1}.	Position assignment
557	Fe-O
879	SiO_2
1627	O-H
1627	C=C
1429	CH_3
2360	C-H

Table 2. Kinetic constants and correlation coefficient.

Pseudo first order				Pseudo-second-order kinetic		
$q_{e,\ expt}$ (mg/L)	$q_{e,cal}$ (mg/L)	k_1 (1/min)	R^2	$q_{e,cal}$ (mg/L)	k_1 (mg/g.min)	R^2
3	1	1.8	0.93	2	0.09	0.96

Table 3. Isotherms study for Dye adsorption

Langmuir isotherm		Freundlich isotherm	
q_m	98	K_f	9
b	7	N	1.3
R^2	0.96	R^2	0.95

ISSN: 2321-9653; IC Value: 45.98; SJ Impact Factor: 7.538
Volume 13 Issue II Feb 2025- Available at www.ijraset.com

Table 4. Comparison study of different adsorbent with adsorption capacity.

Adsorbent	pH	Adsorption capacity (mg/g)	References
α-Fe_2O_3	2-5	16.17	(Dehmani et al., 2020)
Iron impregnated A/C	>7	2.0	(Ge et al., 2018)
Acid modified bentonite	4	6.8	(Ahmadi and Igwegbe, 2018)
Rice husk	7.61	7.89	(Mandal et al., 2019)
Microorganism P. putida and acid-modified CESEP/ZIF-8	-	5.96	(Dong et al., 2020)
Borassus flabellifer fruit husk activated carbon (H_2SO_4 activation)	2	13.42	(Sathya Priya and Sureshkumar, 2020)
Fe_3O_4@GO on silica sand	5	13.97	(Mehmanravesh et al., 2019)
RH+Fe	6	98	Present study

Table 5. Thermodynamic properties dye adsorption at different temperature

Temperature (ºC)	ΔH° (kJ/mol)	ΔS° (kJ/mol)	Ea (KJ /mol)	-ΔG° (KJ/mol)
30	2.9	1.6	1.52	145.2
40				224.6
50				544.5

Highlights

- RH+Fe NPs acts as an excellent adsorbent for dye adsorption because of ion exchange and electrostatic attraction mechanism.
- Dye removal efficiency was achieved 96 % with 60 min by RH+Fe NPs.
- Dye removal parameters on RH+Fe NPs have been optimized.
- Regeneration study showed 82 % removal efficiency till 5^{th} cycle.

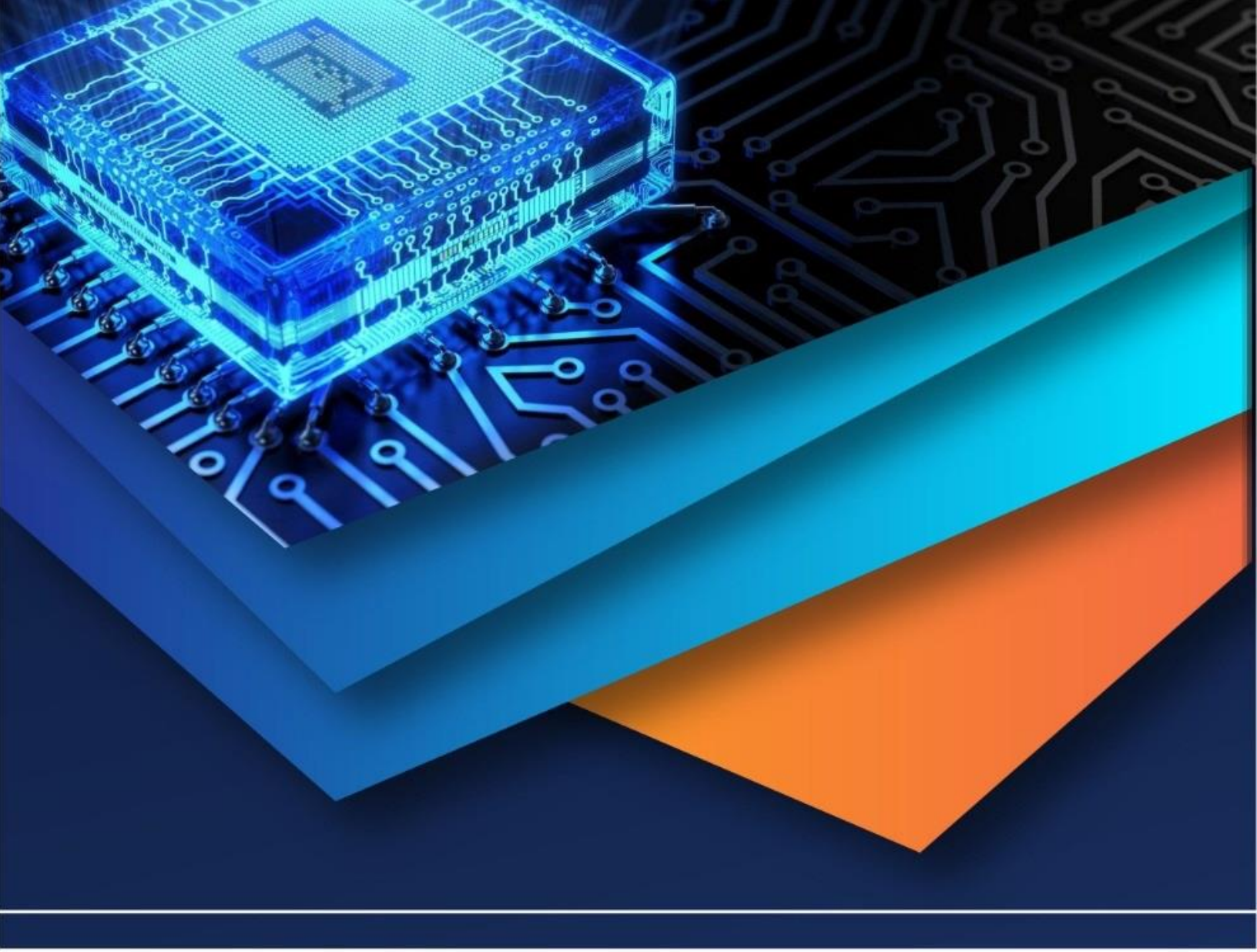

10.22214/IJRASET

45.98

IMPACT FACTOR: 7.129

IMPACT FACTOR: 7.429

INTERNATIONAL JOURNAL FOR RESEARCH

IN APPLIED SCIENCE & ENGINEERING TECHNOLOGY